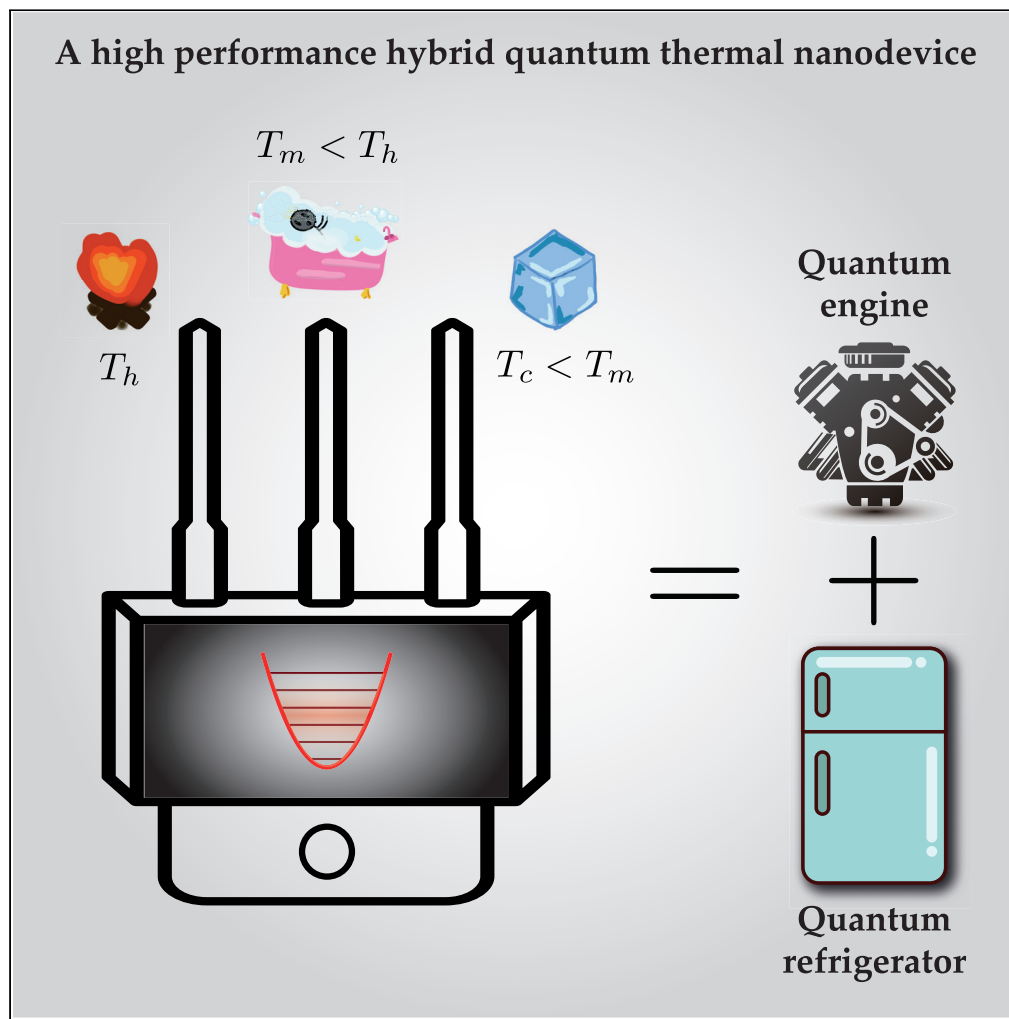


Article

Hybrid quantum thermal machines with dynamical couplings



Fabio Cavaliere,
Luca Razzoli,
Matteo Carrega,
Giuliano Benenti,
Maura Sassetti

giuliano.benenti@uninsubria.it

Highlights

A highly flexible and tunable hybrid thermal machine

High-performance transistor, in terms of output-to-input signal and differential gain



Article

Hybrid quantum thermal machines with dynamical couplings

Fabio Cavaliere,^{1,2} Luca Razzoli,^{3,4} Matteo Carrega,² Giuliano Benenti,^{3,4,5,6,*} and Maura Sassetti^{1,2}

SUMMARY

Quantum thermal machines can perform useful tasks, such as delivering power, cooling, or heating. In this work, we consider hybrid thermal machines, that can execute more than one task simultaneously. We characterize and find optimal working conditions for a three-terminal quantum thermal machine, where the working medium is a quantum harmonic oscillator, coupled to three heat baths, with two of the couplings driven periodically in time. We show that it is possible to operate the thermal machine efficiently, in both pure and hybrid modes, and to switch between different operational modes simply by changing the driving frequency. Moreover, the proposed setup can also be used as a high-performance transistor, in terms of output-to-input signal and differential gain. Owing to its versatility and tunability, our model may be of interest for engineering thermodynamic tasks and for thermal management in quantum technologies.

INTRODUCTION

The fast-paced development of nanoscale technologies is propelling thermodynamics into a new golden era. Just as thermodynamics started in the 1800s spurred by the industrial revolution,¹ in the same way the miniaturization of devices, and in particular the emergence of new quantum technologies, is pushing the field of thermodynamics into new applied and fundamental challenges.^{2–16} Basic questions like the same definitions of work and heat in small systems,^{11,12,17} where quantum mechanics inevitably comes into play, have to be reconsidered with care and are vital to properly characterize the working of nanoscale thermal machines. The minimum temperature achievable in a finite time in small system^{18–21} is not only a fundamental question related to the third law of thermodynamics but also a practical question for cryogenic applications^{10,13} and in the initialization of qubits in a quantum computer.^{22–24} The development of protocols for heat flow control^{13,25} is the key point to evacuate heat and cool hot spots in nanodevices. These are just some of the several fundamental and practical challenges facing thermodynamics. More generally, it has been argued²⁶ that a “quantum energy initiative”, connecting quantum thermodynamics, quantum information science, quantum physics, and engineering, is needed to develop novel, energy-efficient, sustainable quantum technologies.

There is increasing interest in heat engines where a quantum system is coupled to more than just two reservoirs. For instance, in the cooling by heating phenomenon^{27–30} the coupling to a third, photonic reservoir, can be used to extract heat from a cold metal, the refrigeration process being powered by absorption of photons. It has also been shown that a similar setup, with electron transport via a nanostructure bridging two conducting leads and also connected to a third, phonon bath, can be favorable for thermoelectric energy conversion.³¹ Moreover, it has been shown that a third, electronic terminal can improve both the output power and the efficiency at maximum power.^{32–34} In general, a multi-terminal device offers enhanced flexibility that might be useful, for instance, to separate the currents, with charge and heat flowing to different reservoirs.^{35–37} Intriguingly, a three-terminal device can work as a hybrid machine, which performs simultaneously multiple tasks,^{38,39} for instance the heat from a phonon bath could be used to cool one electron terminal and to produce power. On the other hand, three-terminal configurations are standard in the study of thermal transistors, a device whose development is essential for an effective thermal management at the nanoscale.^{40–42}

The above studies of multitasking thermal machines considered stationary conditions, that is, time-independent Hamiltonians and system-bath couplings. On the other hand, driving the system and/or the system-bath couplings offers enhanced design flexibility, and the possibility to switch from some thermodynamic tasks to others simply by tuning the driving frequency. Here, we consider as a working medium (WM) the paradigmatic

¹Dipartimento di Fisica, Università di Genova, Via Dodecaneso 33, 16146 Genova, Italy

²CNR-SPIN, Via Dodecaneso 33, 16146 Genova, Italy

³Center for Nonlinear and Complex Systems, Dipartimento di Scienza e Alta Tecnologia, Università degli Studi dell'Insubria, via Valleggio 11, 22100 Como, Italy

⁴Istituto Nazionale di Fisica Nucleare, Sezione di Milano, via Celoria 16, 20133 Milano, Italy

⁵NEST, Istituto Nanoscienze-CNR, I-56126 Pisa, Italy

⁶Lead contact

*Correspondence: giuliano.benenti@uninsubria.it

<https://doi.org/10.1016/j.isci.2023.106235>



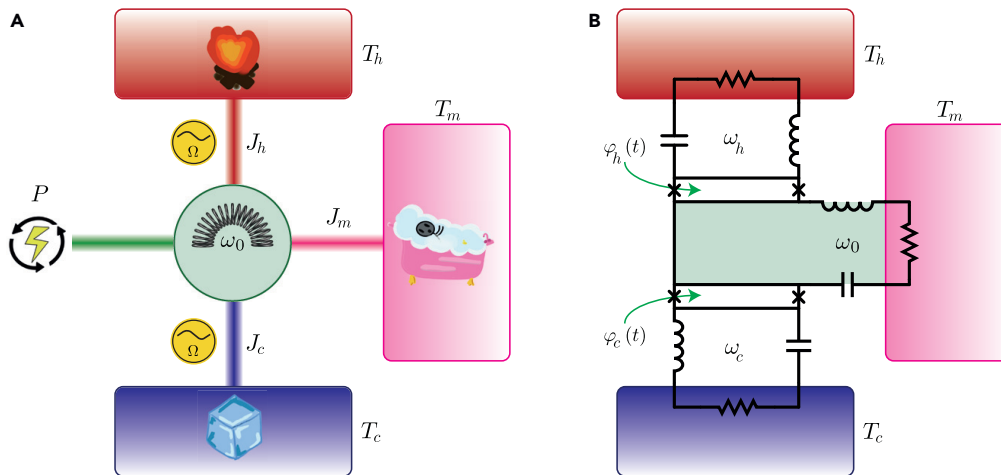


Figure 1. A three-terminal quantum thermal machine

(A) shows a cartoon of a three-terminal setup consisting of a quantum harmonic oscillator (QHO) in contact with three heat baths at temperatures T_ν ($\nu = h, m, c$). The coupling with baths h, c , is dynamical (driven at frequency Ω), whereas bath m is statically connected. Here, J_ν are the energy flows between the QHO and the baths, whereas P is the total power exchanged via the dynamical couplings.

(B) shows a sketch of a possible circuitual implementation: the couplings to baths $\nu = h, c$ are implemented in terms of SQUIDs pierced by harmonically driven fluxes $\varphi_\nu(t)$ (see text for details).

model of a quantum harmonic oscillator (QHO), which represents a basic building block in several quantum technology platforms,^{15,24,43–46} coupled to three thermal reservoirs. We show that by periodically modulating the couplings in a suitable way (see below for details and a physical illustration of our model) it is possible to efficiently run the thermal machine in a pure operation mode (engine, refrigerator, or heat pump), as well as in a hybrid mode, combining two of the above. We also show that it is possible to switch between different operational modes by changing the driving frequency. In addition, we demonstrate that our model can be used as a high-performance transistor, in terms of both output-to-input signal and of differential gain. Finally, we show that the performance of the three-terminal transistor is much better than that achievable with the analogous two-terminal device with modulated coupling.

Model and thermodynamic quantities

Three-terminal thermal machine with dynamical couplings

To study a driven multi-terminal setup that can simultaneously perform several thermodynamic tasks, we focus on the simplest extension beyond the two-terminal paradigm. That is, we consider a three-terminal quantum thermal machine, as sketched in Figure 1A, where the WM is connected to three reservoirs kept at temperatures $T_h > T_m > T_c$. Here, for clarity, we have introduced the subscripts h (“hot”), m (“middle”) and c (“cold”). The temperature T_m may be regarded as an “ambient” (or reference) temperature, to which the system would thermalize if the reservoirs at temperatures $T_{c,h}$ would be disconnected. The total Hamiltonian is

$$H(t) = H_{WM} + \sum_{\nu = h, m, c} [H_\nu + H_{\text{int},\nu}(t)], \quad (\text{Equation 1})$$

where

$$H_{WM} = \frac{p^2}{2M} + \frac{1}{2} M \omega_0^2 x^2, \quad (\text{Equation 2})$$

with M and ω_0 the mass and the characteristic frequency of the QHO, respectively (here and below we set $\hbar = k_B = 1$). To model the ν -th reservoir we adopt a microscopic description of a thermal bath with many degrees of freedom by using the so-called Caldeira-Leggett framework:^{15,47–50} Each reservoir Hamiltonian is described in terms of a collection of independent harmonic oscillators,

$$H_\nu = \sum_{k=1}^{\infty} \left[\frac{P_{k,\nu}^2}{2m_{k,\nu}} + \frac{m_{k,\nu} \omega_{k,\nu}^2 X_{k,\nu}^2}{2} \right], \quad (\text{Equation 3})$$

with $X_{k,\nu}$ and $P_{k,\nu}$ the position and momentum operators of the k -th oscillator of the ν -th bath with associated mass $m_{k,\nu}$ and frequency $\omega_{k,\nu}$, respectively.^{47,49} The interaction between the WM and the ν -th bath,

$$H_{\text{int},\nu}(t) = \sum_{k=1}^{\infty} \left\{ -xg_{\nu}(t)c_{k,\nu}X_{k,\nu} + x^2g_{\nu}^2(t)\frac{c_{k,\nu}^2}{2m_{k,\nu}\omega_{k,\nu}^2} \right\}, \quad (\text{Equation 4})$$

consists of a bilinear coupling between the WM and bath position operators and of the usual counter-term to prevent the renormalization of the WM potential. The interaction strengths are described by the parameter $c_{k,\nu}$, and we have introduced dimensionless functions $g_{\nu}(t)$ that describe the possible time dependence of the couplings. In particular, we will focus on the situation where the $\nu = h, c$ system/bath couplings are modulated in time,^{50–53} whereas the $\nu = m$ coupling is kept constant. Specifically, we assume the two modulations to be in phase, $g_h(t) = g_c(t) = \cos(\Omega t)$, whereas $g_m(t) = 1$. At initial time $t_0 = -\infty$, the total density matrix is assumed factorized as $\rho(t_0) = \rho_{\text{WM}}(t_0) \otimes \rho_h(t_0) \otimes \rho_m(t_0) \otimes \rho_c(t_0)$, with $\rho_{\text{WM}}(t_0)$ the initial WM density matrix, and $\rho_{\nu}(t_0)$ describing the ν -th bath in thermal equilibrium at temperature T_{ν} .

Bath properties can be characterized by the spectral density⁴⁷

$$\mathcal{J}_{\nu}(\omega) = \frac{\pi}{2} \sum_{k=1}^{\infty} \frac{c_{k,\nu}^2}{m_{k,\nu}\omega_{k,\nu}} \delta(\omega - \omega_{k,\nu}), \quad (\text{Equation 5})$$

which encodes memory effects and plays an important role in determining the working regime of thermal machines.^{52,54–57} Hereafter we choose a strictly Ohmic (Note that for strictly Ohmic regime it is assumed the usual bath cut-off ω_c as the largest energy scale, i.e., $\omega_c \gg \omega_0, \Omega$.) spectral density $\mathcal{J}_m(\omega) = M\gamma_m\omega$ for the $\nu = m$ static bath. For the modulated baths $\nu = h, c$, we choose instead a structured environment with a Lorentzian spectral function^{52,58–60}

$$\mathcal{J}_{\nu}(\omega) = \frac{d_{\nu}M\gamma_{\nu}\omega}{(\omega^2 - \omega_{\nu}^2)^2 + \gamma_{\nu}^2\omega^2}, \quad (\text{Equation 6})$$

with a peak centered at ω_{ν} , an amplitude governed by d_{ν} , and a damping width determined by γ_{ν} with $\nu = h, c$. Such structured environments offer a great versatility, i.e., exploiting different resonant conditions between external drive Ω and ω_h and ω_c , and can be physically realized in several settings such as quantum cavity^{44,61} or superconducting circuits.^{45,62–64} In the latter framework, indeed, a QHO can be made by an LC resonator or transmission line, where the phase Φ threaded by the inductor takes the role of the position x , whereas the charge Q accumulated on the capacitors represents the conjugate momentum p , with the standard mapping reviewed in.⁶⁵ There, dissipative elements in the Caldeira-Leggett framework are included by replacing a linear dissipative two-pole element characterized by a frequency dependent admittance $Y(\omega)$ by an infinite set of series-LC oscillators, all wired in parallel. The resulting coupling between the admittance and the quantum system is of the form of Equation 4 where the counter-term arises naturally owing to the potential energy stored in each inductor constituting the bath.⁶⁵ In addition, a structured bath spectral density such as in Equation 6 can be realized by lossy transmission lines.⁶⁶ Therefore, one can think of a device composed of three superconducting LC circuits, one acting as the WM (with an additional resistive coupling toward the $\nu = m$ reservoir) and the other two as transmission lines coupled to baths via capacitive or inductive couplings.^{62,63} The temporal modulation can be engineered by varying a mutual capacitance, or by controlling an inductive coupling via external field after embedding the two LC elements into a superconducting quantum interference device (SQUID)-like geometry as in ref.⁶² Of interest, it has been experimentally demonstrated that the inductive coupling realized by SQUIDs working in the few photon regime can be tuned by an applied magnetic field varying the magnetic flux threading the Josephson junctions.⁶⁷ The presence of this “external knob” allows for a complete tunability of the coupling between resonators (even suppressing/switching-off any direct static couplings). In our setup, the WM is modeled as a quantum harmonic oscillator and therefore it is important to assess in which regime possible nonlinearities of the above implementation may become significant. Indeed, the validity of the harmonic approximation has been investigated^{62,67} and it has been found that it is reasonable in the few ($< 10^3$) photons regime. Our work will focus on the quantum regime (see Sec. results), where $T_{\nu} < \omega_0$ and in which we expect the average occupation number of the QHO to be well within the validity regime of the harmonic approximation. An example of such an implementation is shown in Figure 1B.

In this work, we are interested in thermodynamic quantities in the long time limit, when a periodic steady state has been reached. All quantities of interest are thus averaged over one period of the drive $\mathcal{T} = 2\pi/\Omega$,

and are well defined both at weak and strong couplings.^{53,68–70} The total power and the heat currents, after the quantum ensemble average and averaged over one period of the cycle, read^{51,52}

$$P = \frac{1}{T} \int_{\bar{t}}^{\bar{t}+T} dt' \sum_{\nu=h,c} \text{Tr} \left[\frac{\partial H_{\text{int},\nu}(t')}{\partial t'} \rho(t_0) \right] = \frac{1}{T} \int_{\bar{t}}^{\bar{t}+T} dt' \sum_{\nu=h,c} \text{Tr} \left[\frac{\partial H_{\text{int},\nu}}{\partial t'} \rho(t') \right], \quad (\text{Equation 7})$$

$$J_{\nu} = -\frac{1}{T} \int_{\bar{t}}^{\bar{t}+T} dt' \text{Tr} \left[\frac{d}{dt'} H_{\nu}(t') \rho(t_0) \right] = -\frac{1}{T} \int_{\bar{t}}^{\bar{t}+T} dt' \text{Tr} \left[H_{\nu} \frac{d}{dt'} \rho(t') \right], \quad (\text{Equation 8})$$

where P represents the total power associated with the time evolution of the system/bath couplings $\nu = h, c$ – with $P > 0$ when work is performed on the WM – and J_{ν} is the heat current from the ν -th reservoir, with $J_{\nu} > 0$ when the flow is directed toward the WM, see Figure 1A. We remark here that only the two driven couplings $\nu = h, c$ contribute to the power, because $g_m(t) \equiv 1$.

It is important to notice that the average total power is fully balanced by the average heat currents

$$P + \sum_{\nu=h,m,c} J_{\nu} = 0, \quad (\text{Equation 9})$$

reflecting the First Law of Thermodynamics.^{9,12} Another important quantity to assess thermodynamic performance is the time average entropy production rate, which can be linked to the heat currents by^{9,12,68}

$$\dot{S} = -\sum_{\nu=h,m,c} \frac{J_{\nu}}{T_{\nu}}, \quad (\text{Equation 10})$$

and in terms of which the second law of thermodynamics can be formulated as $\dot{S} \geq 0$. Note that the averaged contribution of the WM to the entropy production vanishes as the system's steady state is periodic with the period of the drive.

Operating modes of a three-terminal thermal machine

The operating modes of a thermal machine can be classified studying the sign of thermal currents and total power. Owing to the energy conservation constraint, $P + J_h + J_c + J_m = 0$, we can express the entropy production rate \dot{S} in terms of the three quantities J_h, J_c and P , thus eliminating the current J_m exchanged with the heat bath at ambient temperature. We then obtain

$$\dot{S} = -\sum_{\nu=h,m,c} \frac{J_{\nu}}{T_{\nu}} = \frac{P}{T_m} + \frac{J_c}{T_m} \left(1 - \frac{T_m}{T_c} \right) + \frac{J_h}{T_m} \left(1 - \frac{T_m}{T_h} \right). \quad (\text{Equation 11})$$

There are 2³ conceivable operating modes: one however is not physical because the combination $J_h < 0, J_c > 0$ and $P < 0$ violates $\dot{S} \geq 0$ – see Equation 11 – and never occurs. The other modes are schematically depicted in Figure 2. One is commonly labeled as “wasteful”^{39,71} because in this configuration $J_c < 0, J_h > 0$ and $P > 0$ – meaning that heat flows from the bath at T_h to the one at T_c while the WM absorbs power. However, this configuration can be a resource for the operation as a thermal transistor, as will be shown in Sec. operation as a thermal transistor. The other six operating modes consist of three “pure” ones (engine, refrigerator, heat pump) and three “hybrid” modes.^{39,72,73} The existence of the latter implies that a three-terminal device can simultaneously perform multiple thermodynamic tasks, such as employing heat from the hot reservoir to produce power (engine) and simultaneously “lift” heat from the cold reservoir (refrigerator), a possibility out of reach for conventional two-terminal thermal machines.^{15,38,39,72,73}

To quantify the performance of a multi-terminal thermal machine in a unified fashion, including also multi-tasking configurations, it is useful to introduce the so-called input–output exergy efficiency, also known as the second-law efficiency or rational efficiency.^{39,72,73} To this end, we split the entropy production rate $\dot{S} = \dot{S}^{(+)} + \dot{S}^{(-)}$ into positive (+) and negative (–) contributions and introduce the exergy efficiency as

$$\phi = -\frac{\dot{S}^{(-)}}{\dot{S}^{(+)}}, \quad (\text{Equation 12})$$

where negative (positive) contributions of the entropy production rate appear in the numerator (denominator). Clearly, because $\dot{S} = \dot{S}^{(+)} - |\dot{S}^{(-)}| \geq 0$, one has $|\dot{S}^{(-)}| \leq \dot{S}^{(+)}$, which implies that $0 \leq \phi \leq 1$. Note that, in simpler cases (e.g., a two-terminal setup operating as an engine), ϕ reduces to the standard

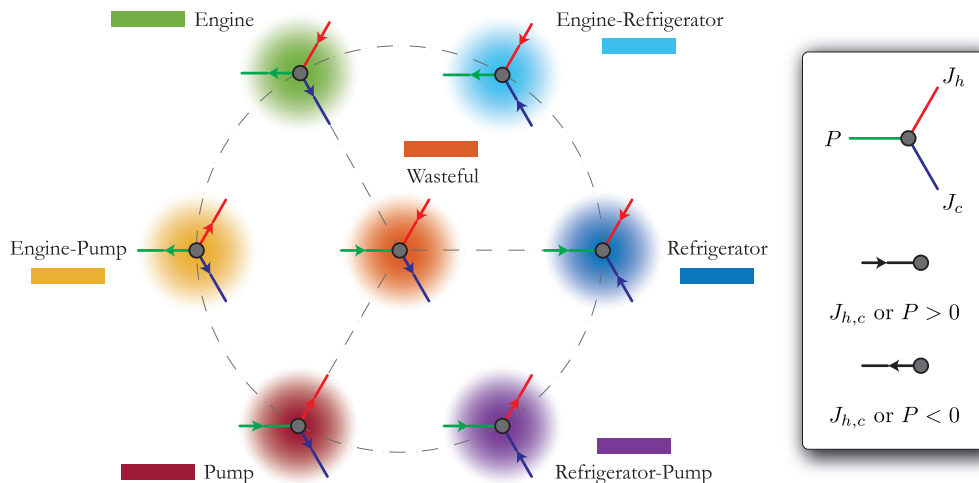


Figure 2. Operating modes of a driven three-terminal device

Schematic depiction of all the possible operating modes of a three-terminal device, as told by the sign of J_h , J_c and P . The dashed lines represent the modes that are connected via the reversal of only one among $J_{h,c}$ or P . The arrows represent the direction of the latter: the relationship with respect to the sign of currents and power is shown in the legend.

thermodynamic efficiency η normalized to the relevant Carnot limit,³⁹ see section “operating modes and thermal transistor effect in a two-terminal device in method details. In our case, using Equation 11, we can write explicitly

$$\phi = -\frac{P\vartheta(-P) + J_c(1 - T_m/T_c)\vartheta(J_c) + J_h(1 - T_m/T_h)\vartheta(-J_h)}{P\vartheta(P) + J_c(1 - T_m/T_c)\vartheta(-J_c) + J_h(1 - T_m/T_h)\vartheta(J_h)}, \quad (\text{Equation 13})$$

where $\vartheta(x)$ is the step function.

RESULTS

We will now present typical results which illustrate the versatility of a three-terminal device, demonstrating in particular its ability to perform hybrid tasks. In addition, we will show that the same setup can be configured as a useful thermal transistor.^{13,74–78} Hereafter, we consider the quantum regime¹³

$$\omega_0 > T_h > T_m > T_c. \quad (\text{Equation 14})$$

We focus on the perturbative regime in which the coupling with the driven Lorentzian baths is much smaller than the one with the static Ohmic bath. The amplitude d_ν (for $\nu = h, c$) in Equation 6 can be expressed in terms of the dimensionless parameter

$$\kappa_\nu = \frac{d_\nu}{\omega_\nu^2 \omega_0^2} \ll 1. \quad (\text{Equation 15})$$

As for the other parameters of the Lorentzian baths, we assume that their resonant frequencies $\omega_{h,c} > 0$ can be independently tuned, with the detuning parameter $\Delta = \omega_h - \omega_c$, and that the widths $\gamma_h = \gamma_c$. Finally, we address the underdamped regime with $\gamma_\nu \ll \omega_0$, in which the machine can display its best performances. In these conditions compact analytical expressions can be obtained^{51,52} for the thermal currents J_ν and power P : they are reported in section thermal currents and power in the perturbative regime in method details, see Equations 22 and 23.

Operation as a hybrid device

The three-terminal quantum device proposed here can display several different operating modes. To maximize their number, we have found that choosing $\Delta > 0$ is a key ingredient (see below for an explanation of this observation). Figures 3A and 3B show the operating mode of the device as a function of Ω and ω_h with a large detuning $\Delta = 0.75\omega_0$, for two representative values of the middle temperature T_m . When $T_m \sim T_h$ (panel A) we encounter a very rich scenario characterized by all the pure modes with the refrigerator-pump and pump-engine hybrid behaviors. It is important to stress that this last regime cannot be observed with only two terminals, see section operating modes and thermal transistor effect in a two-terminal device in

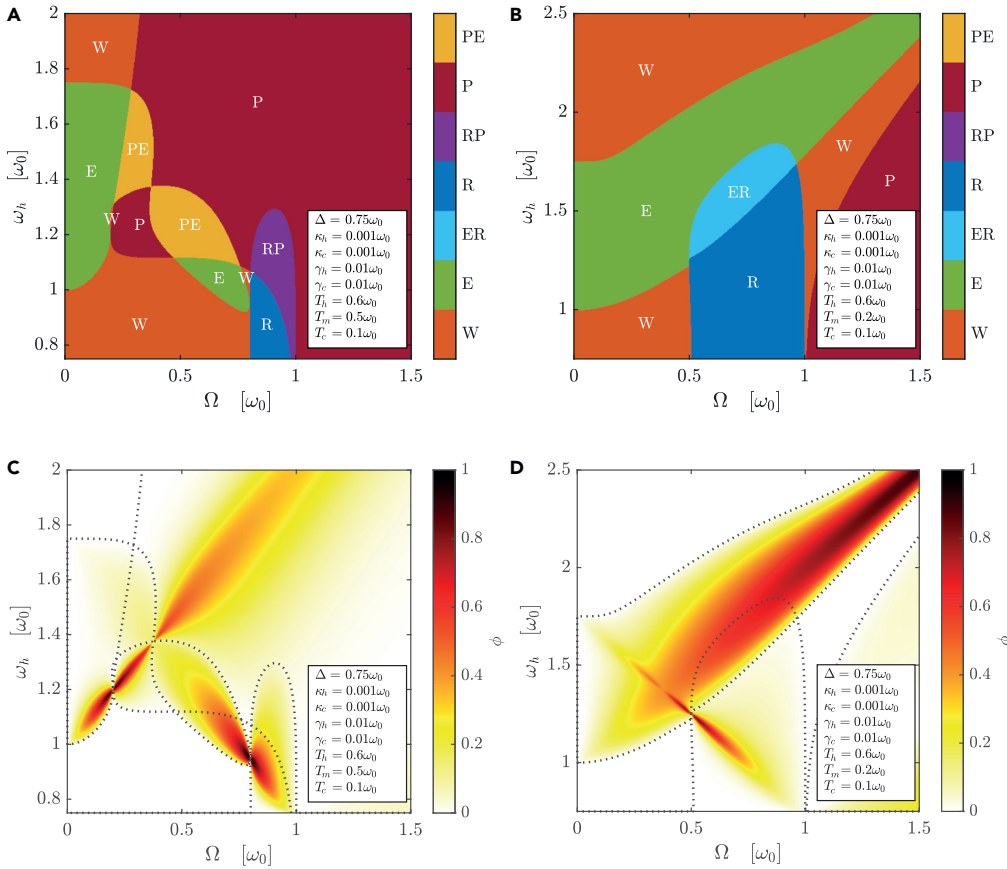


Figure 3. Hybrid operation of a three-terminal device

(A–D) Operating modes (A and B) and corresponding exergy efficiency ϕ (C and D) as a function of the driving frequency Ω and ω_h for a three-terminal quantum thermal machine operating with same parameters except for $T_m = 0.5\omega_0$ in panels (A and C) and $T_m = 0.2\omega_0$ in panels (B and D). Here we recall that $\Delta = \omega_h - \omega_c$.

method details. Considering instead $T_m \sim T_c$, exemplified by panel (B), we still observe a varied (but somewhat simpler) scenario, which however features the engine–refrigerator hybrid operation, which again is lacking in the two-terminal device. A very intriguing feature of our system is its ability to seamlessly switch between several different modes of choice by tuning ω_h , Δ and, more simply, using the external driving frequency Ω as a control knob. As an example, considering the situation in panel (A) and $\omega_h \approx 1.5\omega_0$ it is in principle possible to switch back and forth between engine, a hybrid engine-heat pump and a heat pump by sweeping Ω in a range $\leq 0.5\omega_0$. Similar configurations are of course possible by choosing different regions of the parameter space. Importantly, most of the configurations are quite wide with respect to ω_h and do not depend sensibly on the specific value of Δ , which suggests that the operation and the tunability of device are quite stable and robust.

Figures 3C and 3D show the exergy efficiency ϕ as a function of Ω and ω_h for the same parameters of panels (A) and (B) discussed above. Clearly, $\phi = 0$ in the wasteful regions. Away from them, the exergy efficiency can attain significant values ≥ 0.5 both in the pure as well as in the hybrid modes. One feature clearly stands out: the largest values of ϕ occur around two precise lines in the Ω , ω_h plane. This is because the three-terminal device can be seen as two two-terminal devices in parallel: the machine \mathcal{M}_1 operating between T_m and $T_h > T_m$, and \mathcal{M}_2 working between T_c and $T_m > T_c$. The behavior of such a two-terminal device has been analyzed previously,⁵² see section **operating modes and thermal transistor effect in a two-terminal device** in **method details** for a brief summary. In particular, the two high-efficiency lines mentioned above correspond to the resonances $\omega_h = \omega_0 + \Omega$, owing to the operation of \mathcal{M}_1 and $\omega_c = \omega_0 - \Omega = \omega_h - \Delta$, because of the operation of \mathcal{M}_2 . This observation also allows us to understand the richness of panels (A) and (B), owing to the superposition of the different working modes of the “elementary” two-terminal

devices in terms of which the three-terminal one can be interpreted. Such superposition occurs if $\omega_c < \omega_h$ which implies $\Delta > 0$, which reveals why this is a favorable regime to observe hybrid operating modes. [Figure S2A](#) in the [supplemental information](#) shows a typical situation found when $\Delta < 0$ and confirms the disappearance of hybrid modes.

Operation as a thermal transistor

Three-terminal quantum thermal devices have been envisioned as possible templates to implement a quantum thermal transistor,^{13,42,71,77} i.e., a device in which a small modulation of an energy flow (a “input”, analogous to the gate/base of an electronic transistor) produces a large modulation of another, larger energy flow (a “output”, similar for instance to the source/emitter in a conventional transistor).⁷⁷ Typical setups considered in literature consist of several two-level-systems (TLS) statically coupled to external baths.⁴² There, the modulation of the “input” flow is provided by a modulation of the temperature of the “input” bath (typically, corresponding to the one at temperature T_m). The periodic modulation of one of the TLSs has been also considered.⁷⁷ Proposals of a thermal transistor in a two-terminal device with parametric excitation have also been put forward:⁷⁶ the two terminals serve the purpose of source/emitter and drain/collector, whereas the exchanged power with the parametric actuator serves as the gate/base. In such a transistor the modulation of the gate is achieved via the modulation of the frequency of the parametric excitation, which offers the practical advantage of being simpler to achieve in a precise manner in comparison to the modulation of the temperature of a bath. In this work we endorse this idea, and show that a three-terminal quantum thermal transistor with remarkable performances and stability can be achieved in our setup, which outperforms an analogous device with only two terminals.

We consider the exchanged power P , modulated through the driving frequency Ω of the dynamical couplings, as the input, and the current J_h flowing from the hot bath as the output. Similar results (not shown) can be obtained considering J_c as the output. We introduce

$$r = \left| \frac{J_h}{P} \right|; g = \left| \frac{\partial J_h}{\partial P} \right| = \left| \frac{\partial J_h / \partial \Omega}{\partial P / \partial \Omega} \right|. \quad (\text{Equation 16})$$

The parameter r controls the output-to-input ratio, i.e., the “smallness” of the input signal with respect to the output, whereas g represents the differential gain of the transistor, i.e., the amplification factor of small changes in P , reflected on J_h . We chose to customarily set a performance threshold, by considering a “useful” transistor a device in which both $r > 10$ and $g > 10$ is achieved, and performed a search scanning the parameters space. [Figure 4A](#) shows a typical case in which the three-terminal device indeed works as a quantum thermal transistor: both criteria are met, and a gain up to $\sim 10^4$ can indeed be achieved. The performance is stable, with the region in Ω over which $r, g > 10$ extending over a frequency range $\geq 0.5\omega_0$. We have found (not shown) that to achieve solid and robust transistor action, the best condition occurs with minimal detuning of the two Lorentzian baths $\Delta \approx 0$, with $T_m \approx T_c$. To put this result in context with the different operating modes of the device, [Figure 4B](#) shows the region in parameter space where the device operates as a transistor as a solid black segment, superimposed to a plot of ϕ where the different operating modes are marked. The best transistor regimes are found near the boundaries between the “re-entrant” wasteful-engine-wasteful operating modes, where P switches sign two times (see [Figure 2](#)) while J_h preserves it. This clearly drives r to very large values near the inversion points of P . It is found that in these regions P is also sufficiently smooth with respect to Ω , which in turn allows us to obtain a large gain g . With no detuning, the exergy efficiency ϕ is found to be weak, reaching at most 0.4 (in contrast with [Figure 3](#), where $\Delta \neq 0$ and ϕ can approach the ideal unit efficiency). However, in the case of a thermal transistor a trade-off between ϕ and r, g seems acceptable because in this regime the device is not intended to perform as a conventional thermal machine.

In our setup, the performance of a three-terminal transistor is far superior to that of a two-terminal device operating in the same manner and within the same temperature range – obtained for instance switching off the coupling $g_c(t) = 0$ – for which the figures of merit r and g can be defined as in [Equation 16](#). The results for this two-terminal transistor, shown in [Figure S1D](#) in the [supplemental information](#), clearly show that the driving range where a significant gain is achieved is much narrower, extending up to a frequency window of about $0.15\omega_0$: operating with three terminals warrants a definite advantage in terms of the stability of the thermal transistor.

We have also analyzed the situation in which the transistor operates with P as the input and J_h as the output, but keeping Ω fixed and modulating the temperature T_m – see [Figure S2B](#) in the [supplemental information](#),

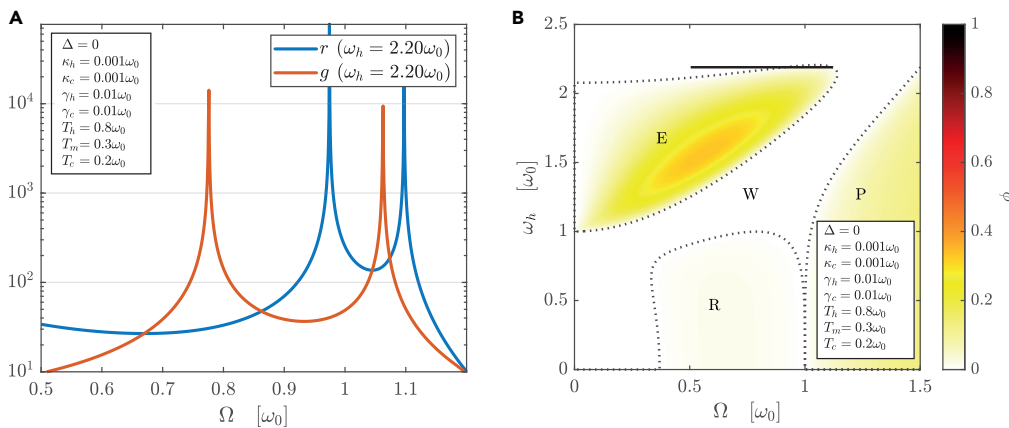


Figure 4. Three-terminal device as a quantum thermal transistor

(A) shows the output-to-input ratio r and differential gain g as a function of Ω , for a set of parameters chosen to optimize the range of driving frequencies where the system performs as a thermal transistor.

(B) shows such range (as a thick solid line), superimposed to a density plot of the exergy efficiency ϕ as a function of Ω and ω_h .

obtained for a set of parameters optimizing its performances. In this case the differential gain is independent of T_m but remains lower (by more than an order of magnitude) than the peak values obtained modulating Ω . As far as the output-to-input ratio is concerned, it achieves values similar to those obtained modulating the driving frequency, with a overall smooth behavior. Such a configuration may be useful if a very linear amplifier is sought, trading off the gain magnitude and the greater flexibility offered by modulating Ω .

DISCUSSION AND CONCLUSIONS

We have shown that by properly engineering bath spectral features and driving the system-bath couplings, a three-terminal quantum thermal machine can act as an efficient hybrid thermal machine. The proposed device is flexible and tunable, in that several pure and hybrid working modes can be obtained, and it is possible to switch from one operational mode to another by changing the driving frequency. Moreover, the same device can work as a stable, high-performance transistor, with large output-to-input signal and differential gain, on a broad driving frequency interval.

Natural extensions of our model could be obtained by considering hybrid quantum thermal machines with more complex working medium, like coupled oscillators or qubit-oscillator systems. It would be also interesting to consider the coupling to non-equilibrium reservoirs, which may be a useful resource for further boosting the performance of hybrid quantum thermal machines. Also, connecting multiple quantum thermal transistors to produce more complex and flexible quantum thermal circuits would be an interesting perspective, as also recently suggested,^{79,80} possibly leading to the implementation of a fully controllable quantum thermal logic.⁸¹

Finally our analysis reported average quantities, whereas fluctuations, ubiquitous at the nanoscale, can influence device performance, but also provide alternative pathway in developing new device functionalities. In particular, the so-called thermodynamic uncertainty relations, constraining in classical stochastic thermodynamics the achievable degree of precision (i.e., the minimum fluctuations in the outcome of a process), given a certain output power and efficiency,^{82,83} deserve further careful inspection in the quantum realm.

Limitations of the study

The study is exact in the limit where the involved systems (working medium and environment) are harmonic. For the sake of simplicity, we assume the perturbative regime where the coupling with the Lorentzian baths is weak.

STAR★METHODS

Detailed methods are provided in the online version of this paper and include the following:

- KEY RESOURCES TABLE
- RESOURCE AVAILABILITY
 - Lead contact
 - Materials availability
 - Data and code availability
- METHOD DETAILS
 - Thermal currents and power in the perturbative regime
 - Operating modes and thermal transistor effect in a two-terminal device

SUPPLEMENTAL INFORMATION

Supplemental information can be found online at <https://doi.org/10.1016/j.isci.2023.106235>.

ACKNOWLEDGMENTS

F.C. and M.S. acknowledge support by the “Dipartimento di Eccellenza MIUR 2018–2022.”, L.R. and G.B. acknowledge financial support by the Julian Schwinger Foundation (Grant JSF-21-04-0001) and by INFN through the project ‘QUANTUM’. F.C. acknowledges support by V. Cavaliere for the preparation of Figure 1.

AUTHOR CONTRIBUTIONS

F.C., L.R., and M.C. performed analytical calculations and numerical simulations. M.S. conceived and supervised the study, with inputs from G.B. All authors discussed the results and contributed to writing and revising the manuscript.

DECLARATION OF INTERESTS

The authors declare no competing interests.

Received: November 29, 2022

Revised: January 31, 2023

Accepted: February 15, 2023

Published: January 18, 2023

REFERENCES

1. Clausius, R. (1867). *The Mechanical Theory of Heat – with its Applications to the Steam Engine and to the Physical Properties of Bodies* (J. Van Voorst, London). <https://doi.org/10.1088/0957-4484/26/3/032001>.
2. Esposito, M., Harbola, U., and Mukamel, S. (2009). Nonequilibrium fluctuations, fluctuation theorems, and counting statistics in quantum systems. *Rev. Mod. Phys.* *81*, 1665. <https://doi.org/10.1103/RevModPhys.81.1665>.
3. Campisi, M., Hänggi, P., and Talkner, P. (2011). *Colloquium: quantum fluctuation relations: foundations and applications*. *Rev. Mod. Phys.* *83*, 771–791. <https://doi.org/10.1103/RevModPhys.83.771>.
4. Kosloff, R. (2013). Quantum thermodynamics: a dynamical viewpoint. *Entropy* *15*, 2100–2128. <https://doi.org/10.3390/e15062100>.
5. Gelbwaser-Klimovsky, D., Niedenzu, W., and Kurizki, G. (2015). Thermodynamics of quantum systems under dynamical control. In *Advances In Atomic, Molecular, and Optical Physics*, 64, E. Arimondo, C.C. Lin, and S.F. Yelin, eds. (Academic Press), pp. 329–407. <https://doi.org/10.1016/bs.aamop.2015.07.002>.
6. Sothmann, B., Sánchez, R., and Jordan, A.N. (2015). Thermoelectric energy harvesting with quantum dots. *Nanotechnology* *26*, 032001. <https://doi.org/10.1088/0957-4484/26/3/032001>.
7. Vinjanampathy, S., and Anders, J. (2016). Quantum thermodynamics. *Contemp. Phys.* *57*, 545–579. <https://doi.org/10.1080/00107514.2016.1201896>.
8. Goold, J., Huber, M., Riera, A., del Rio, L., and Skrzypczyk, P. (2016). The role of quantum information in thermodynamics—a topical review. *J. Phys. A: Math. Theor.* *49*, 143001. <https://doi.org/10.1088/1751-8113/49/14/143001>.
9. Benenti, G., Casati, G., Saito, K., and Whitney, R. (2017). Fundamental aspects of steady-state conversion of heat to work at the nanoscale. *Phys. Rep.* *694*, 1–124. <https://doi.org/10.1016/j.physrep.2017.05.008>.
10. Fornieri, A., and Giazotto, F. (2017). Towards phase-coherent caloritronics in superconducting circuits. *Nat. Nanotechnol.* *12*, 944–952. <https://doi.org/10.1038/nnano.2017.204>.
11. Talkner, P., and Hänggi, P. (2020). *Colloquium: statistical mechanics and thermodynamics at strong coupling: quantum and classical*. *Rev. Mod. Phys.* *92*, 041002. <https://doi.org/10.1103/RevModPhys.92.041002>.
12. Landi, G.T., and Paternostro, M. (2021). Irreversible entropy production: from classical to quantum. *Rev. Mod. Phys.* *93*, 035008. <https://doi.org/10.1103/RevModPhys.93.035008>.
13. Pekola, J.P., and Karimi, B. (2021). *Colloquium: quantum heat transport in condensed matter systems*. *Rev. Mod. Phys.* *93*, 041001. <https://doi.org/10.1103/RevModPhys.93.041001>.
14. Landi, G.T., Poletti, D., and Schaller, G. (2022). Nonequilibrium boundary-driven quantum systems: Models, methods, and properties. *Rev. Mod. Phys.* *94*, 045006. <https://doi.org/10.1103/RevModPhys.94.045006>.
15. Arrachea, L. (2023). Energy dynamics, heat production and heat-work conversion with qubits: toward the development of quantum machines. *Rep. Progr. Phys.* *86*, 036501. <https://doi.org/10.1088/1361-6633/acb06b>.
16. Piccitto, G., Campisi, M., and Rossini, D. (2022). The Ising critical quantum Otto engine. *New J. Phys.* *24*, 103023. <https://doi.org/10.1088/1367-2630/ac963b>.
17. Esposito, M., Lindenberg, K., and Van den Broeck, C. (2010). Entropy production as correlation between system and reservoir.

- New J. Phys. 12, 013013. <https://doi.org/10.1088/1367-2630/12/1/013013>.
18. Levy, A., Alicki, R., and Kosloff, R. (2012). Quantum refrigerators and the third law of thermodynamics. *Phys. Rev. E Stat. Nonlin. Soft Matter Phys.* 85, 061126. <https://doi.org/10.1103/PhysRevE.85.061126>.
 19. Benenti, G., and Strini, G. (2015). Dynamical Casimir effect and minimal temperature in quantum thermodynamics. *Phys. Rev. A* 91, 020502(R). <https://doi.org/10.1103/PhysRevA.91.020502>.
 20. Freitas, N., and Paz, J.P. (2017). Fundamental limits for cooling of linear quantum refrigerators. *Phys. Rev. E* 95, 012146. <https://doi.org/10.1103/PhysRevE.95.012146>.
 21. Clivaz, F., Silva, R., Haack, G., Brask, J.B., Brunner, N., and Huber, M. (2019). Unifying paradigms of quantum refrigeration: a universal and attainable bound on cooling. *Phys. Rev. Lett.* 123, 170605. <https://doi.org/10.1103/PhysRevLett.123.170605>.
 22. Benenti, G., Casati, G., Rossini, D., and Strini, G. (2019). *Principles of Quantum Computation and Information (A Comprehensive Textbook)* (World Scientific).
 23. Krantz, P., Kjaergaard, M., Yan, F., Orlando, T.P., Gustavsson, S., and Oliver, W.D. (2019). A quantum engineer's guide to superconducting qubits. *Appl. Phys. Rev.* 6, 021318. <https://doi.org/10.1063/1.5089550>.
 24. Calzona, A., and Carrega, M. (2023). Multi-mode architectures for noise-resilient superconducting qubits. *Supercond. Sci. Technol.* 36, 023001. <https://doi.org/10.1088/1361-6668/aca64>.
 25. José Martínez-Pérez, M., and Giazotto, F. (2014). A quantum diffractor for thermal flux. *Nat. Commun.* 5, 3579. <https://doi.org/10.1038/ncomms4579>.
 26. Auffèves, A. (2022). Quantum technologies need a quantum energy initiative. *PRX Quant.* 3, 020101. <https://doi.org/10.1103/PRXQuantum.3.020101>.
 27. Pekola, J.P., and Hekking, F.W.J. (2007). Normal-metal-superconductor tunnel junction as a brownian refrigerator. *Phys. Rev. Lett.* 98, 210604. <https://doi.org/10.1103/PhysRevLett.98.210604>.
 28. Cleuren, B., Rutten, B., and Van den Broeck, C. (2012). Cooling by heating: refrigeration powered by photons. *Phys. Rev. Lett.* 108, 120603. <https://doi.org/10.1103/PhysRevLett.108.120603>.
 29. Mari, A., and Eisert, J. (2012). Cooling by heating: very hot thermal light can significantly cool quantum systems. *Phys. Rev. Lett.* 108, 120602. <https://doi.org/10.1103/PhysRevLett.108.120602>.
 30. Naseem, M.T., and Müstecaplıoğlu, Ö.E. (2021). Ground-state cooling of mechanical resonators by quantum reservoir engineering. *Commun. Phys.* 4, 95. <https://doi.org/10.1038/s42005-021-00599-z>.
 31. Jiang, J.-H., Entin-Wohlman, O., and Imry, Y. (2012). Thermoelectric three-terminal hopping transport through one-dimensional nanosystems. *Phys. Rev. B* 85, 075412. <https://doi.org/10.1103/PhysRevB.85.075412>.
 32. Mazza, F., Bosisio, R., Benenti, G., Giovannetti, V., Fazio, R., and Taddei, F. (2014). Thermoelectric efficiency of three-terminal quantum thermal machines. *New J. Phys.* 16, 085001. <https://doi.org/10.1088/1367-2630/16/8/085001>.
 33. Yang, J., Elouard, C., Splettstoesser, J., Sothmann, B., Sánchez, R., and Jordan, A.N. (2019). Thermal transistor and thermometer based on Coulomb-coupled conductors. *Phys. Rev. B* 100, 045418. <https://doi.org/10.1103/PhysRevB.100.045418>.
 34. Blasi, G., Taddei, F., Arrachea, L., Carrega, M., and Braggio, A. (2020). Nonlocal thermoelectricity in a topological Andreev interferometer. *Phys. Rev. B* 102, 241302. <https://doi.org/10.1103/PhysRevB.102.241302>.
 35. Mazza, F., Valentini, S., Bosisio, R., Benenti, G., Giovannetti, V., Fazio, R., and Taddei, F. (2015). Separation of heat and charge currents for boosted thermoelectric conversion. *Phys. Rev. B* 91, 245435. <https://doi.org/10.1103/PhysRevB.91.245435>.
 36. Sánchez, R., Sothmann, B., and Jordan, A.N. (2015). Heat diode and engine based on quantum Hall edge states. *New J. Phys.* 17, 075006. <https://doi.org/10.1088/1367-2630/17/7/075006>.
 37. Thierschmann, H., Sánchez, R., Sothmann, B., Arnold, F., Heyn, C., Hansen, W., Buhmann, H., and Molenkamp, L.W. (2015). Three-terminal energy harvester with coupled quantum dots. *Nat. Nanotechnol.* 10, 854–858. <https://doi.org/10.1038/nnano.2015.176>.
 38. Entin-Wohlman, O., Imry, Y., and Aharony, A. (2015). Enhanced performance of joint cooling and energy production. *Phys. Rev. B* 91, 054302. <https://doi.org/10.1103/PhysRevB.91.054302>.
 39. Manzano, G., Sánchez, R., Silva, R., Haack, G., Brask, J.B., Brunner, N., and Potts, P.P. (2020). Hybrid thermal machines: generalized thermodynamic resources for multitasking. *Phys. Rev. Res.* 2, 043302. <https://doi.org/10.1103/PhysRevResearch.2.043302>.
 40. Li, B., Wang, L., and Casati, G. (2006). Negative differential thermal resistance and thermal transistor. *Appl. Phys. Lett.* 88, 143501. <https://doi.org/10.1063/1.2191730>.
 41. Li, N., Ren, J., Wang, L., Zhang, G., Hänggi, P., and Li, B. (2012). *Colloquium: phononics: Manipulating heat flow with electronic analogs and beyond*. *Rev. Mod. Phys.* 84, 1045–1066. <https://doi.org/10.1103/RevModPhys.84.1045>.
 42. Joulain, K., Drevillon, J., Ezzahri, Y., and Ordóñez-Miranda, J. (2016). Quantum thermal transistor. *Phys. Rev. Lett.* 116, 200601. <https://doi.org/10.1103/PhysRevLett.116.200601>.
 43. Blais, A., Huang, R.-S., Wallraff, A., Girvin, S.M., and Schoelkopf, R.J. (2004). Cavity quantum electrodynamics for superconducting electrical circuits: an architecture for quantum computation. *Phys. Rev. A* 69, 062320. <https://doi.org/10.1103/PhysRevA.69.062320>.
 44. Aspelmeyer, M., Kippenberg, T.J., and Marquardt, F. (2014). Cavity optomechanics. *Rev. Mod. Phys.* 86, 1391–1452. <https://doi.org/10.1103/RevModPhys.86.1391>.
 45. Cottet, A., Dartailh, M.C., Desjardins, M.M., Cubaynes, T., Contamin, L.C., Delbecq, M., Viennot, J.J., Bruhat, L.E., Douçot, B., and Kontos, T. (2017). Cavity QED with hybrid nanocircuits: from atomic-like physics to condensed matter phenomena. *J. Phys. Condens. Matter* 29, 433002. <https://doi.org/10.1088/1361-648X/aa7b4d>.
 46. Zhang, W.-M., Lo, P.-Y., Xiong, H.-N., Tu, M.W.-Y., and Nori, F. (2012). General non-Markovian dynamics of open quantum systems. *Phys. Rev. Lett.* 109, 170402. <https://doi.org/10.1103/PhysRevLett.109.170402>.
 47. Weiss, U. (2021). *Quantum Dissipative Systems – 5th Edition* (World Scientific).
 48. Hu, B.L., Paz, J.P., and Zhang, Y. (1992). Quantum Brownian motion in a general environment: exact master equation with nonlocal dissipation and colored noise. *Phys. Rev. D: Part. Fields* 45, 2843–2861. <https://doi.org/10.1103/PhysRevD.45.2843>.
 49. Caldeira, A.O., and Leggett, A.J. (1983). Quantum tunnelling in a dissipative system. *Ann. Phys. (N. Y.)* 149, 374–456. [https://doi.org/10.1016/0003-4916\(83\)90202-6](https://doi.org/10.1016/0003-4916(83)90202-6).
 50. Cangemi, L.M., Carrega, M., De Candia, A., Cataudella, V., De Filippis, G., Sassetti, M., and Benenti, G. (2021). Optimal energy conversion through antiadiabatic driving breaking time-reversal symmetry. *Phys. Rev. Res.* 3, 013237. <https://doi.org/10.1103/PhysRevResearch.3.013237>.
 51. Carrega, M., Cangemi, L.M., De Filippis, G., Cataudella, V., Benenti, G., and Sassetti, M. (2022). Engineering dynamical couplings for quantum thermodynamic tasks. *PRX Quant.* 3, 010323. <https://doi.org/10.1103/PRXQuantum.3.010323>.
 52. Cavaliere, F., Carrega, M., De Filippis, G., Cataudella, V., Benenti, G., and Sassetti, M. (2022). Dynamical heat engines with non-Markovian reservoirs. *Phys. Rev. Res.* 4, 033233. <https://doi.org/10.1103/PhysRevResearch.4.033233>.
 53. Wiedmann, M., Stockburger, J.T., and Ankerhold, J. (2020). Non-Markovian dynamics of a quantum heat engine: out-of-equilibrium operation and thermal coupling control. *New J. Phys.* 22, 033007. <https://doi.org/10.1088/1367-2630/ab725a>.
 54. Breuer, H.-P., Laine, E.-M., Piilo, J., and Vacchini, B. (2016). *Colloquium: non-Markovian dynamics in open quantum systems*. *Rev. Mod. Phys.* 88, 021002. <https://doi.org/10.1103/RevModPhys.88.021002>.
 55. Iles-Smith, J., Lambert, N., and Nazir, A. (2014). Environmental dynamics, correlations, and the emergence of noncanonical equilibrium states in open quantum systems.

- Phys. Rev. A 90, 032114. <https://doi.org/10.1103/PhysRevA.90.032114>.
56. Gröblacher, S., Trubarov, A., Prigge, N., Cole, G.D., Aspelmeyer, M., and Eisert, J. (2015). Observation of non-Markovian micromechanical Brownian motion. *Nat. Commun.* 6, 7606. <https://doi.org/10.1038/ncomms8606>.
57. Torre, G., Roga, W., and Illuminati, F. (2015). Non-markovianity of Gaussian channels. *Phys. Rev. Lett.* 115, 070401. <https://doi.org/10.1103/PhysRevLett.115.070401>.
58. Strasberg, P., Schaller, G., Lambert, N., and Brandes, T. (2016). Nonequilibrium thermodynamics in the strong coupling and non-Markovian regime based on a reaction coordinate mapping. *New J. Phys.* 18, 073007. <https://doi.org/10.1088/1367-2630/18/7/073007>.
59. Restrepo, S., Cerrillo, J., Strasberg, P., and Schaller, G. (2018). From quantum heat engines to laser cooling: floquet theory beyond the Born–Markov approximation. *New J. Phys.* 20, 053063. <https://doi.org/10.1088/1367-2630/aac583>.
60. Naseem, M.T., Misra, A., Müstecaplıoğlu, Ö.E., and Kurizki, G. (2020). Minimal quantum heat manager boosted by bath spectral filtering. *Phys. Rev. Res.* 2, 033285. <https://doi.org/10.1103/PhysRevResearch.2.033285>.
61. Teufel, J.D., Donner, T., Li, D., Harlow, J.W., Allman, M.S., Cicak, K., Sirois, A.J., Whittaker, J.D., Lehnert, K.W., and Simmonds, R.W. (2011). Sideband cooling of micromechanical motion to the quantum ground state. *Nature* 475, 359–363. <https://doi.org/10.1038/nature10261>.
62. Peropadre, B., Zueco, D., Wulfschner, F., Deppe, F., Marx, A., Gross, R., and García-Ripoll, J.J. (2013). Tunable coupling engineering between superconducting resonators: from sidebands to effective gauge fields. *Phys. Rev. B* 87, 134504. <https://doi.org/10.1103/PhysRevB.87.134504>.
63. Rodrigues, I.C., Bothner, D., and Steele, G.A. (2019). Coupling microwave photons to a mechanical resonator using quantum interference. *Nat. Commun.* 10, 5359. <https://doi.org/10.1038/s41467-019-12964-2>.
64. Luschmann, T., Schmidt, P., Deppe, F., Marx, A., Sanchez, A., Gross, R., and Huebl, H. (2022). Mechanical frequency control in inductively coupled electromechanical systems. *Sci. Rep.* 12, 1608. <https://doi.org/10.1038/s41598-022-05438-x>.
65. Vool, U., and Devoret, M. (2017). Introduction to quantum electromagnetic circuits. *Int. J. Circ. Theor. Appl.* 45, 897–934. <https://doi.org/10.1002/cta.2359>.
66. Hofer, P.P., Souquet, J.-R., and Clerk, A.A. (2016). Quantum heat engine based on photon-assisted Cooper pair tunneling. *Phys. Rev. B* 93, 041418. <https://doi.org/10.1103/PhysRevB.93.041418>.
67. Wulfschner, F., Goetz, J., Koessel, F.R., Hoffmann, E., Baust, A., Eder, P., Fischer, M., Haeberlein, M., Schwarz, M.J., Pernpeintner, M., et al. (2016). Tunable coupling of transmission-line microwave resonators mediated by an rf SQUID. *EPJ Quant. Technol.* 3, 10. <https://doi.org/10.1140/epjqt/s40507-016-0048-2>.
68. Ptaszyński, K., and Esposito, M. (2019). Entropy production in open systems: the predominant role of intraenvironment correlations. *Phys. Rev. Lett.* 123, 200603. <https://doi.org/10.1103/PhysRevLett.123.200603>.
69. Liu, J., Jung, K.A., and Segal, D. (2021). Periodically driven quantum thermal machines from warming up to limit cycle. *Phys. Rev. Lett.* 127, 200602. <https://doi.org/10.1103/PhysRevLett.127.200602>.
70. Brandner, K., and Seifert, U. (2016). Periodic thermodynamics of open quantum systems. *Phys. Rev. E* 93, 062134. <https://doi.org/10.1103/PhysRevE.93.062134>.
71. Hajiloo, F., Sánchez, R., Whitney, R.S., and Splettstoesser, J. (2020). Quantifying nonequilibrium thermodynamic operations in a multiterminal mesoscopic system. *Phys. Rev. B* 102, 155405. <https://doi.org/10.1103/PhysRevB.102.155405>.
72. Lu, J., Wang, Z., Wang, R., Peng, J., Wang, C., and Jiang, J.-H. (2023). Multitask quantum thermal machines and cooperative effects. *Phys. Rev. B* 107, 075428. <https://doi.org/10.1103/PhysRevB.107.075428>.
73. López, R., Lim, J.S., and Kim, K.W. (2023). Optimal superconducting hybrid machine. *Phys. Rev. Research* 5, 013038. <https://doi.org/10.1103/PhysRevResearch.5.013038>.
74. Dutta, B., Peltonen, J.T., Antonenko, D.S., Meschke, M., Skvortsov, M.A., Kubala, B., König, J., Winkelmann, C.B., Courtois, H., and Pekola, J.P. (2017). Thermal conductance of a single-electron transistor. *Phys. Rev. Lett.* 119, 077701. <https://doi.org/10.1103/PhysRevLett.119.077701>.
75. Gubaydullin, A., Thomas, G., Golubev, D.S., Lvov, D., Peltonen, J.T., and Pekola, J.P. (2022). Photonic heat transport in three terminal superconducting circuit. *Nat. Commun.* 13, 1552. <https://doi.org/10.1038/s41467-022-29078-x>.
76. Riera-Campeny, A., Mehboudi, M., Pons, M., and Sanpera, A. (2019). Dynamically induced heat rectification in quantum systems. *Phys. Rev. E* 99, 032126. <https://doi.org/10.1103/PhysRevE.99.032126>.
77. Gupt, N., Bhattacharya, S., Das, B., Datta, S., Mukherjee, V., and Ghosh, A. (2022). Floquet quantum thermal transistor. *Phys. Rev. E* 106, 024110. <https://doi.org/10.1103/PhysRevE.106.024110>.
78. Ligato, N., Paolucci, F., Strambini, E., and Giazotto, F. (2022). Thermal superconducting quantum interference proximity transistor. *Nat. Phys.* 18, 627–632. <https://doi.org/10.1038/s41567-022-01578-z>.
79. Wijesekara, R.T., Gunapala, S.D., and Premaratne, M. (2022). Towards quantum thermal multi-transistor systems: energy divider formalism. *Phys. Rev. B* 105, 235412. <https://doi.org/10.1103/PhysRevB.105.235412>.
80. Wijesekara, R.T., Gunapala, S.D., and Premaratne, M. (2021). Darlington pair of quantum thermal transistors. *Phys. Rev. B* 104, 045405. <https://doi.org/10.1103/PhysRevB.104.045405>.
81. Paolucci, F., Marchegiani, G., Strambini, E., and Giazotto, F. (2018). Phase-tunable thermal logic: computation with heat. *Phys. Rev. Appl.* 10, 024003. <https://doi.org/10.1103/PhysRevApplied.10.024003>.
82. Pietzonka, P., and Seifert, U. (2018). Universal trade-off between power, efficiency, and constancy in steady-state heat engines. *Phys. Rev. Lett.* 120, 190602. <https://doi.org/10.1103/PhysRevLett.120.190602>.
83. Horowitz, J.M., and Gingrich, T.R. (2019). Thermodynamic uncertainty relations constrain non-equilibrium fluctuations. *Nat. Phys.* 16, 15–20. <https://doi.org/10.1038/s41567-019-0702-6>.
84. Zerbe, C., and Hänggi, P. (1995). Brownian parametric quantum oscillator with dissipation. *Phys. Rev. E Stat. Phys. Plasmas Fluids Relat. Interdiscip. Topics* 52, 1533–1543. <https://doi.org/10.1103/PhysRevE.52.1533>.
85. Freitas, N., and Paz, J.P. (2018). Cooling a quantum oscillator: a useful analogy to understand laser cooling as a thermodynamical process. *Phys. Rev. A* 97, 032104. <https://doi.org/10.1103/PhysRevA.97.032104>.
86. Arrachea, L., Mucciolo, E.R., Chamon, C., and Capaz, R.B. (2012). Microscopic model of a phononic refrigerator. *Phys. Rev. B* 86, 125424. <https://doi.org/10.1103/PhysRevB.86.125424>.
87. Buffoni, L., Solfanelli, A., Verrucchi, P., Cuccoli, A., and Campisi, M. (2019). Quantum measurement cooling. *Phys. Rev. Lett.* 122, 070603. <https://doi.org/10.1103/PhysRevLett.122.070603>.
88. Solfanelli, A., Falsetti, M., and Campisi, M. (2020). Nonadiabatic single-qubit quantum Otto engine. *Phys. Rev. B* 101, 054513. <https://doi.org/10.1103/PhysRevB.101.054513>.

STAR★METHODS

KEY RESOURCES TABLE

REAGENT or RESOURCE	SOURCE	IDENTIFIER
Software and algorithms		
MATLAB R2022b	The MathWorks, Inc.	https://www.mathworks.com
Wolfram Mathematica 12.2	Wolfram Research, Inc.	https://www.wolfram.com/mathematica/

RESOURCE AVAILABILITY

Lead contact

Further information and requests for resources should be directed to the lead contact, Giuliano Benenti (giuliano.benenti@uninsubria.it).

Materials availability

This study did not generate new unique materials.

Data and code availability

- All data have been numerically generated. All calculations can be carried out using the equations presented in the main text and using, e.g., the softwares listed in the [key resources table](#).
- This paper does not report original code.
- Any additional information required to reanalyze the data reported in this paper is available from the [lead contact](#) upon reasonable request.

METHOD DETAILS

Thermal currents and power in the perturbative regime

The driven dissipative three-terminal setup described in the main text can be solved by resorting to non-equilibrium Green function formalism, as described in ref.⁵¹ Here, we briefly recall the main steps for the evaluation of thermodynamic quantities of interest, referring to previous literature for additional details. From the total Hamiltonian in [Equation 1](#) one can derive the equations of motion for the WM variables ($x(t)$, $p(t)$) and baths variables ($X_{k,\nu}(t)$, $P_{k,\nu}(t)$). The solution for the latter degrees of freedom can be expressed in terms of initial conditions and of the operator $x(t)$,^{20,51,84,85} eventually obtaining a generalized quantum Langevin equation of the form

$$\ddot{x}(t) + \omega_0^2 x(t) + \int_{-\infty}^{+\infty} ds \sum_{\nu=h,m,c} g_{\nu}(t) \gamma_{\nu}(t-s) [\dot{g}_{\nu}(s)x(s) + \dot{x}(s)g_{\nu}(s)] = \frac{1}{M} \sum_{\nu=h,m,c} g_{\nu}(t) \xi_{\nu}(t),$$

(Equation 17)

where the overdots denote time derivatives, we recall that $g_m(t) \equiv 1$, the damping kernels $\gamma_{\nu}(t)$ are linked to the spectral function by

$$\gamma_{\nu}(t) = \frac{2}{\pi M} \vartheta(t) \int_0^{\infty} d\omega \frac{\mathcal{J}_{\nu}(\omega)}{\omega} \cos(\omega t),$$

(Equation 18)

and $\xi_{\nu}(t)$ represent the fluctuating force operators of the baths with $\vartheta(t)$ the Heaviside step function. We recall that these operators have zero quantum average $\langle \xi_{\nu}(t) \rangle \equiv \text{Tr}[\xi_{\nu}(t)\rho(t_0)] = 0$ and their time correlators are given by $\langle \xi_{\nu}(t)\xi_{\nu'}(t') \rangle = \delta_{\nu,\nu'} \mathcal{L}_{\nu}(t-t')$, with

$$\mathcal{L}_{\nu}(t) = \int_0^{\infty} \frac{d\omega}{\pi} \mathcal{J}_{\nu}(\omega) \left[\coth\left(\frac{\omega}{2T_{\nu}}\right) \cos(\omega t) - i \sin(\omega t) \right].$$

(Equation 19)

At long times, the system reaches a periodic state sustained by the drives. In this regime, the time evolution of the position operator $x(t)$ can be expressed directly as a time integral of the retarded Green function with the inhomogeneous term

$$x(t) = \sum_{\nu=h,m,c} \int_{-\infty}^{+\infty} dt' G(t, t') \frac{1}{M} g_{\nu}(t') \xi_{\nu}(t'). \quad (\text{Equation 20})$$

Several methods can be used to evaluate (exactly or with different approximation schemes) the above Green function, see e.g. Ref.^{20,51,52,86}

From Equations 7 and 8, it is possible to express both the power and the heat currents averaged over one period T in terms of position variables as

$$P = \int_{\bar{t}}^{\bar{t}+T} \frac{dt'}{T} \left\{ \sum_{\nu=h,c} -\dot{g}_{\nu}(t') \langle x(t') \xi_{\nu}(t') \rangle + M \dot{g}_{\nu}(t') \int_{-\infty}^{+\infty} ds \gamma_{\nu}(t' - s) \frac{d}{ds} [g_{\nu}(s) \langle x(t') x(s) \rangle] \right\} \quad (\text{Equation 21})$$

and

$$J_{\nu} = \int_{\bar{t}}^{\bar{t}+T} \frac{dt'}{T} \left[-\frac{g_{\nu}(t')}{2} \langle x(t') \dot{\xi}_{\nu}(t') + \dot{\xi}_{\nu}(t') x(t') \rangle - g_{\nu}(t') \int_{-\infty}^{t'} ds \langle \{x(t'), x(s)\} \rangle g_{\nu}(s) \right. \\ \left. \int_0^{\infty} \frac{d\omega}{\pi} \mathcal{J}_{\nu}(\omega) \omega \cos(\omega(t' - s)) \right],$$

with $\{A, B\} = AB + BA$ the standard anti-commutator. It is worth to note that the average power gets contributions only from the two driven couplings $\nu = h, c$, since $\nu = m$ is kept constant with $g_m(t) = 1$.

In this work we are interested in the weak coupling regime, where the driven bath couplings ($\nu = h, c$) are much weaker than the static one ($\nu = m$). In this case, closed analytical expressions for average power and heat currents can be obtained in a standard perturbative framework.⁵² In the regime $\gamma_m \ll \omega_0$, the final expressions read (for $\nu = h, c$)

$$J_{\nu} = \frac{1}{4M\omega_0} \sum_{\rho=\pm 1} (\omega_0 + \rho\Omega) \mathcal{J}_{\nu}(\omega_0 + \rho\Omega) \left[n_B \left(\frac{\omega_0 + \rho\Omega}{T_{\nu}} \right) - n_B \left(\frac{\omega_0}{T_m} \right) \right], \quad (\text{Equation 22})$$

$$P = -\frac{\Omega}{4M\omega_0} \sum_{\nu=h,c,p=\pm 1} p \mathcal{J}_{\nu}(\omega_0 + p\Omega) \left[n_B \left(\frac{\omega_0 + p\Omega}{T_{\nu}} \right) - n_B \left(\frac{\omega_0}{T_m} \right) \right], \quad (\text{Equation 23})$$

where $n_B(x) = (e^x - 1)^{-1}$ is the Bose function and we note that Equations 22 and 23 do not depend anymore on γ_m for $\gamma_m \ll \omega_0$.⁵² We do not quote the expression for J_m as it can be derived from the conservation of energy in Equation 9.

Operating modes and thermal transistor effect in a two-terminal device

In this section we briefly discuss the operation of a two-terminal quantum thermal machine with a QHO as the WM, operating between a Lorentzian bath with dynamical coupling and a static Ohmic bath.⁵² The theoretical framework can be derived from the material in Sec. [model and thermodynamic quantities](#), for vanishing coupling to one of the two Lorentzian baths.

The operating modes of a two-terminal device can be characterized with the same criteria shown in [Figure 2](#). We denote the hot and cold baths as T_h and $T_c < T_h$. A general landscape of all the possible operating modes is shown in [Figure S1](#) in the [supplemental information](#) where panel (A) displays the case where the Lorentzian bath is at temperature T_h , and panel (C) illustrates the case of a Lorentzian bath at temperature T_c . These two cases correspond respectively to the machines \mathcal{M}_1 and \mathcal{M}_2 discussed in Sec. [operation as a hybrid device](#).

The only achievable modes here are the two pure "engine" and "heat pump" modes, the hybrid "refrigerator-pump" mode, and the "wasteful" mode. In passing, we note that other works^{52,87,88} use different names for such operating modes: there, the terms "refrigerator", "dissipator" and "accelerator" correspond to "refrigerator-pump", "heat pump" and "wasteful" used here. Due to the presence of a sharply peaked Lorentzian bath, the machine displays its most prominent features when the resonance conditions $\omega_h = \omega_0 + \Omega$ (for the machine \mathcal{M}_1) or $\omega_c = \omega_0 - \Omega$ (for the machine \mathcal{M}_2) are met.⁵² These resonances are marked as a white dashed line in [Figures S1A](#) and [S1C](#) in the [supplemental information](#). The presence of

such resonances is quite evident in the behavior of the exergy efficiency, shown in [Figure S1B](#) for the case of \mathcal{M}_1 (the situation for \mathcal{M}_2 is qualitatively identical). The latter quantity simplifies considerably in the two-terminal case, where the energy balance relation reads

$$P + J_h + J_c = 0. \quad (\text{Equation 24})$$

For a heat engine the relevant quantities are $P < 0$, $J_h > 0$ and the efficiency $\eta = |P|/J_h$. Exploiting [Equation 24](#), the entropy production rate can be rewritten as

$$\dot{S} = \frac{P + J_h}{T_c} - \frac{J_h}{T_h} = \frac{P}{T_c} + J_h \left(\frac{1}{T_c} - \frac{1}{T_h} \right), \quad (\text{Equation 25})$$

where the first term on the last passage is negative ($P < 0$), while the second is positive. Hence recalling the definition of exergy, we can write

$$\phi = \frac{|P|}{J_h} \frac{1}{1 - T_c/T_h} = \frac{\eta}{\eta_C}, \quad (\text{Equation 26})$$

with $\eta_C = 1 - T_c/T_h$ the Carnot limit for the engine efficiency. Similarly, it can be shown that the same holds for a two-terminal refrigerator. In this case, the relevant quantities are $P > 0$, $J_c > 0$ and the coefficient of performance (CoP) $\epsilon = J_c/P$. We can write

$$\dot{S} = J_c \left(\frac{1}{T_h} - \frac{1}{T_c} \right) + \frac{P}{T_h}, \quad (\text{Equation 27})$$

where the first term is negative (since $J_c > 0$) and the second is positive. The exergy efficiency for a two-terminal refrigerator is thus

$$\phi = \frac{J_c}{P} \left(\frac{T_h}{T_c} - 1 \right) = \frac{\epsilon}{\epsilon_C}, \quad (\text{Equation 28})$$

where $\epsilon_C = T_c/(T_h - T_c)$ is the Carnot limit of the CoP. The highest values of ϕ occur near the resonance line, with $\phi \rightarrow 1$ near the intersection between the resonance line and the line separating the engine and the refrigerator-pump regimes, where $P \rightarrow 0$.

Finally, [Figure S1D](#) in the [supplemental information](#) shows the typical best-case scenario concerning the performances of a thermal transistor built out of a two-terminal device operating within a temperature range analogous to that of [Figure 4](#): clearly the range of driving frequencies where a useful gain $g > 10$ is achieved is only of about $0.15\omega_0$, considerably smaller than the one obtained in the three-terminal case. This general trend has always been observed throughout all our investigations.